EGU 2018-11222E

Dynamic pressure effects on the geospace system: Global MHD simulation and observations

Dogacan Su Ozturk*, Shasha Zou, James A. Slavin, Aaron J. Ridley
University of Michigan, Department of Climate and Space Sciences and Engineering
contact: dcsoztrk@umich.edu

1.INTRODUCTION AND OBJECTIVES

The changes in the solar wind dynamic pressure can perturb the geospace system significantly. Traditionally studied with ground magnetometers, the dynamic pressure enhancement signatures are named as **positive SIs (SI^+)** and the pressure drop signatures are named as **negative SIs (SI^-)**.The response of the geospace system to dynamic pressure drops are not as commonly studied as the enhancement events. Araki and Nagano [1988] were the first to examine ground magnetometer response to presssure decrement events. They suggested that the ground magnetometer signatures for SI^-s should be opposite to the ones derived for compression events shown in Figure 1 [Araki, 1994].

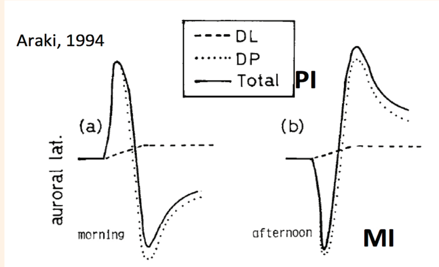

Figure 1: The SI signal at different locations recorded by ground magnetometers [Araki, 1994].

The SI^- studies gained further significance when Sato et al. [2001] showed that expansion events can trigger substorms. Consequent modeling studies have showed the relaxation events consisted of a two step response equivalent to the **Preliminary Impulse (PI)** and the **Main Impulse (MI)** in compression events. Observations of magnetospheric flows indicated magnetospheric vortices gave rise to MI^- signatures, which had opposite sense of rotations to those formed during compression as shown in Figure 2. However the exact source for the PI^- signature is still not well understood.

The aim of this study is to understand the response of the geospace system to negative impulse events by answering the following questions:
- What are the sources for the negative PI and MI signatures?
- How do these perturbations affect the Ionosphere-Thermosphere system?
- How do the negative pressure impulse events compare to positive impulse events?

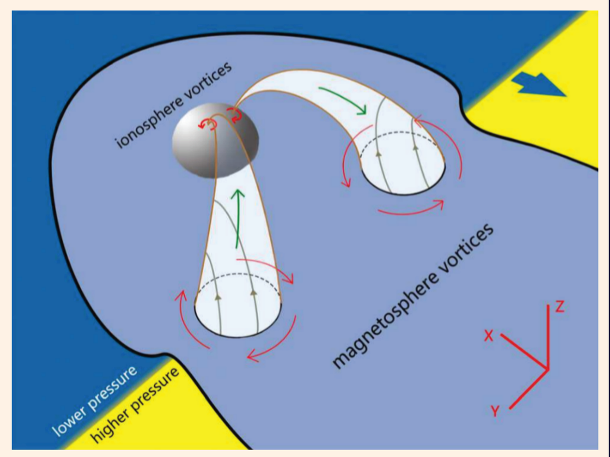

Figure 2: The magnetospheric vortices and their ionospheric counterparts that form during a negative pressure impulse event [Zhao et al., 2016].

2.METHODOLOGY

To understand the global geospace system response, the University of Michigan Space Weather Modeling Framework (SWMF) has been used. The model was driven with solar wind plasma and Interplanetary Magnetic Field (IMF) measurements obtained from OMNI Database. Three modules are used to specify the global magnetosphere which are Global Magnetosphere (GM), Inner Magnetosphere (IM) and Ionospheric Electrodynamics modules. We used **Rice Convection Model (RCM)** for IM and **Ridley Ionosphere Model (RIM)** for IE modules. The high resolution output from the IE module was later used to drive the Global Ionosphere Thermosphere Model (GITM). The IE driver has **1°(latitude)x1°(longitude) spatial resolution and 10 s temporal resolution**. We also included **600 virtual ground magnetometers at each hemisphere** to study the magnetic signatures of the event on the ground.

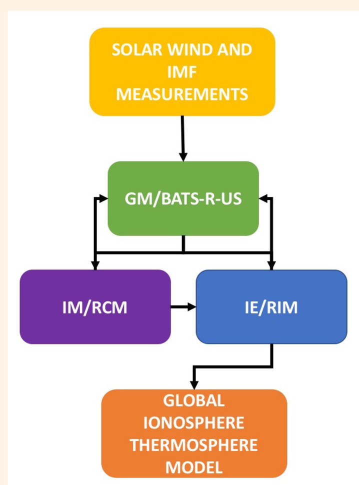

Figure 3: A diagram showing the different models and their coupling used in this study.

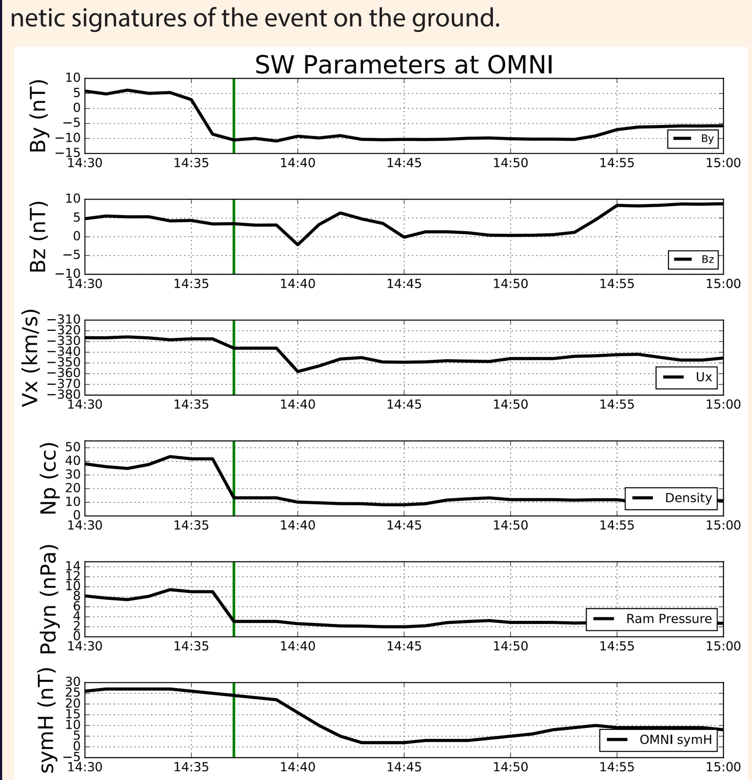

Figure 4: The values of IMF B_Y, IMF B_Z, solar wind velocity V_X, solar wind density N_P, solar wind dynamic pressure P_{dyn} and sym-H index between 1430 UT- 1500 UT are shown for the 11 June 2017 event. The vertical green line shows the arrival of negative pressure pulse at 14237 UT. The measurements are taken from OMNI Database.

The 11 June 2017 event was simulated to study the negative pressure impulse event. The OMNI observations are shown in Figure 4. The negative pressure impulse arrives at **1437 UT**. At the time of event:
- IMF B_Y turns from positive to negative.
- IMF B_Z is positive but turns southward for a brief period around 1440 UT.
- The dynamic pressure drops from **9 nPa to 3 nPa**. This drop was mainly due to the solar wind density drop from 42 cc to 14 cc.
- The solar wind velocity was slightly enhanced during this period.
- Sym-H index did not show a significant response to pressure drop before 1440 UT.

3. GROUND MAGNETOMETER RESPONSE

We compared the virtual magnetometers results of the N component with the HOP magnetometer at Hopen Island [lat=76°N , lon=25°E] and RAN magnetometer at Rankine Inlet [lat=62°N , lon=92°W]. The HOP magnetometer was at the dusk sector [16.5 MLT, 74° latitude] and the RAN magnetometer was at the dawn sector [8 MLT, 72° latitude] during the event.
The **dusk** magnetometer recorded **a peak** while the **dawn** magnetometer recorded **a dip** during the negative PI phase. Consequently, the **dusk** magnetometer recorded **a dip** while the **dawn** magnetometer recorded **a peak** during the negative MI phase. The virtual magnetometers recorded similar trends despite **the lower magnitudes**.
The SI^- produced opposite PI and MI signatures to that of a SI^+ event indicating there were **two pairs of perturbation** currents with opposite directions to those formed during a compression event.

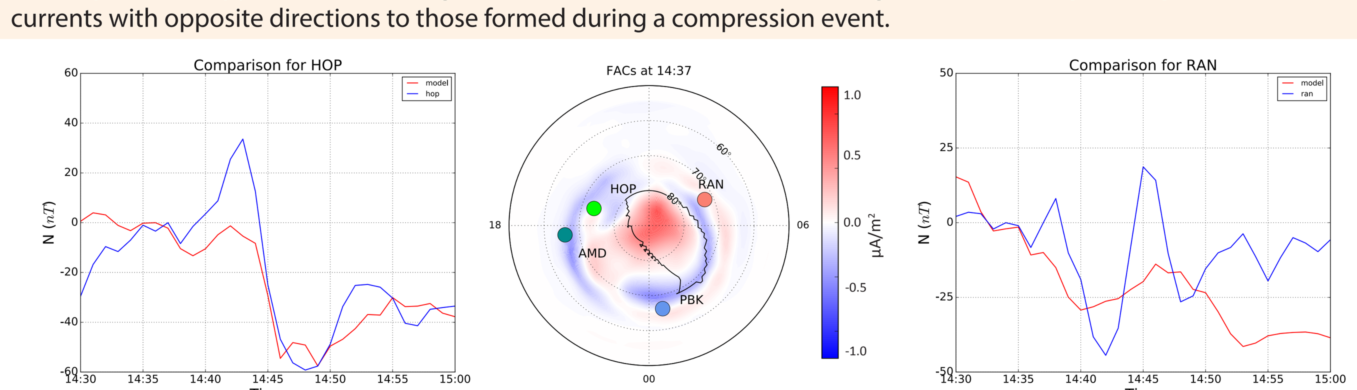

Figure 5: The comparison of the N component of the magnetic perturbations recorded by HOP and RAN magnetometers are shown in blue at the left and right panels between 1430 - 1500 UT, while the red lines show the virtual ground magnetometer response at these locations. The middle panel shows the FACs at 1437 UT and the locations of select ground magnetometer stations in MLT coordinates.

4. RESPONSE OF THE NORTHERN HEMISPHERE

The time evolution of the Ionosphere system at the Northern hemisphere is shown in Figure 5. The Field Aligned Currents (FACs), the perturbation FACs, the N component of the magnetic perturbation, the Joule heating profile due to perturbations, ion temperature profile at 227km with ion convection flow vectors and the Hall conductance profiles are shown for the period between 1437 UT to 1447 UT. The panels a,b,c,d and f were results from the IE/RIM module and they are shown in MLT coordinates. The panel-e shows the results in geographic coordinates from GITM which are driven by using the solutions from IE/RIM module.

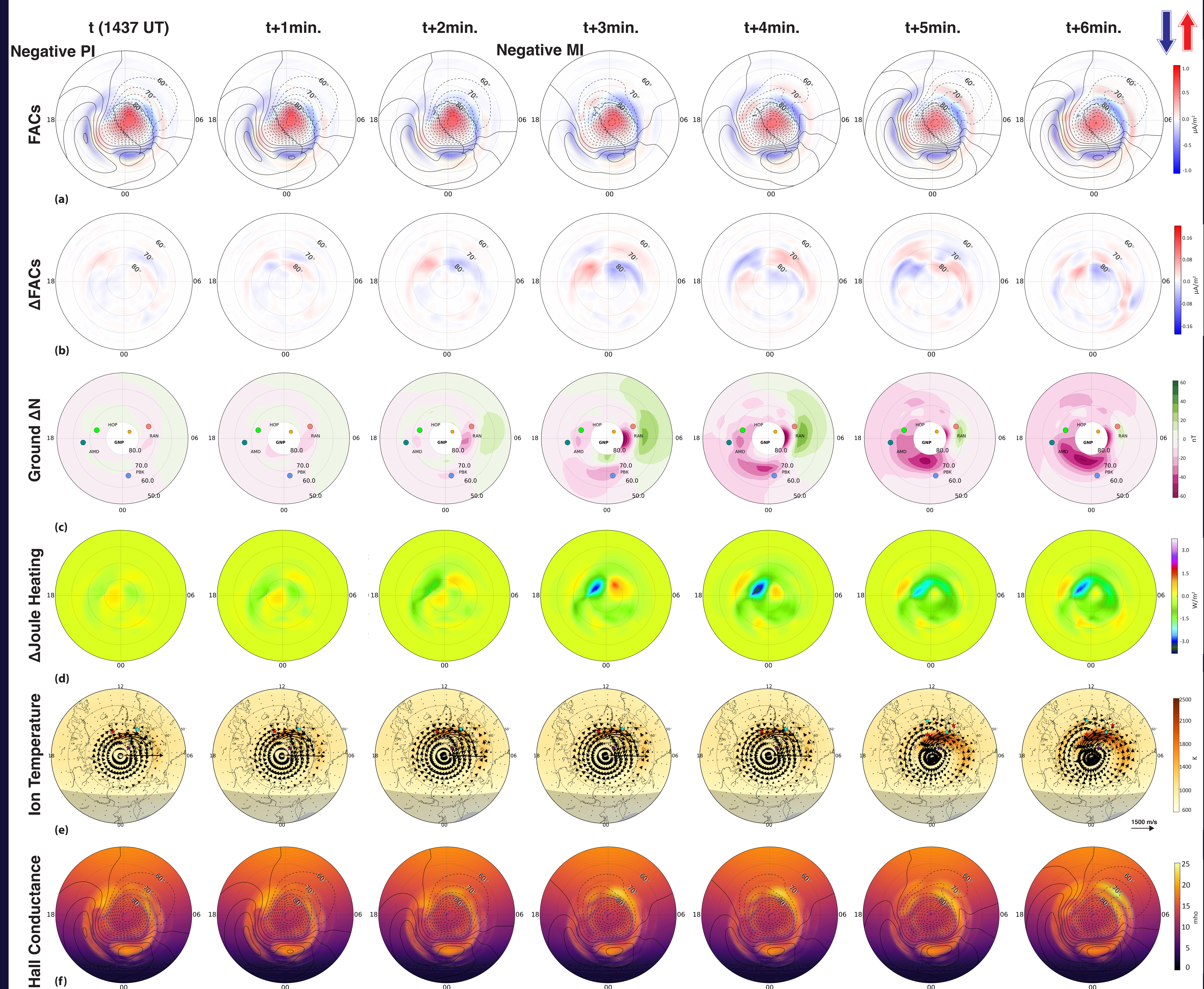

Figure 6: The FACs (a), running dfferenced FACs (b), N component of the baseline subtracted ground magnetic perturbations (c), baseline subtracted Joule heating profile (d), ion temperature profile with ion convection vectors (e) and the hall conductance profile (f) are shown in 7 time steps between 1437 UT to 1444 UT. Locations of the ground magnetometers are plotted on Panel-c. Panel-e is in the geographic local time and the blue (red) stars mark the peak of differenced downward (upward) perturbation FACs.

The negative PI phase:

Between 1437 UT-1439 UT, a perturbation FAC that was **upward on dusk and downward on dawn** has formed and propagated to higher latitudes. The dawn magnetometers recorded a drop in the N component, while the dusk magnetometers showed an enhancement in this interval. There were mild enhancements in the Joule heating profile, especially in the dawn region. The ion convection profile was not significantly perturbed but ion temperature enhancements in the order of **400 K** were recorded. The Hall conductance profile did not show a significant change.

The negative MI phase:

Between 1440UT-1444UT, a new perturbation FAC formed on the negative PI FAC system, which was **upward on dawn and downward on dusk**. The dawn magnetometers recorded an enhancement, whereas the dusk magnetometers recorded a drop in the N component. The Joule heating profile enhanced at dawn and decreased at dusk, similar to the Hall conductance profile. The ion convection profile extended to lower latitudes but not a significant change was seen on the ion temperatures before 1443 UT.

The effects of southward turning IMF B_Z:

The brief southward turnin of the IMF B_Z particularla disturbed the ion convection system, creating strong return flows between 9-11 Local times at high latitudes, at the time of event the ion temperature showed an enhancement around 700 K.

5. MAGNETOSPHERIC RESPONSE

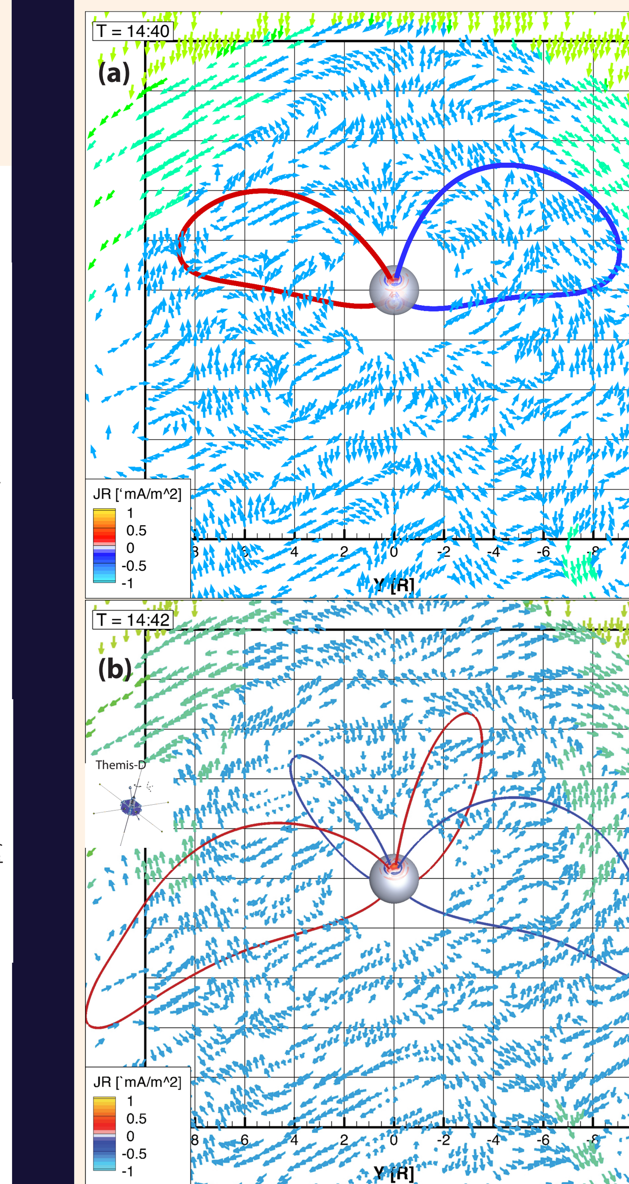

Figure 7: The magnetospheric flow profiles at 1440 UT (a) and 1442 UT (b) are shown. The flow vectors are colored based on the velocity. The magnetic field lines that map to the center of the flow vortices are plotted and colored based on the direction of the FAC they map to on the top of the ionosphere.

Negative PI Phase:

During the negative PI phase, the magnetosphere started expanding. **Sunward flows** ocured on the dayside and two vortices, a **clockwise rotating vortex** associated with a downward FAC at dawn, and a **counter clockwise rotating vortex** associated with an upward FAC at dusk formed.

Negative MI Phase:

During the negative MI phase, another pair of vortices formed with **opposite senses of rotation** to the negative PI vortices. A clockwise rotating vortex associated with a downward FAC formed on the dusk and a counter clockwise rotating vortex associated with an upward FAC formed on the dawn.
The values extracted from the simulation along the Themis-D track showed a similar clockwise rotating vortex at the same location. However, the location of Themis-D corresponded to the coarser grid on the simulation domain. Therefore the virtual satellite results showed a larger vortex.

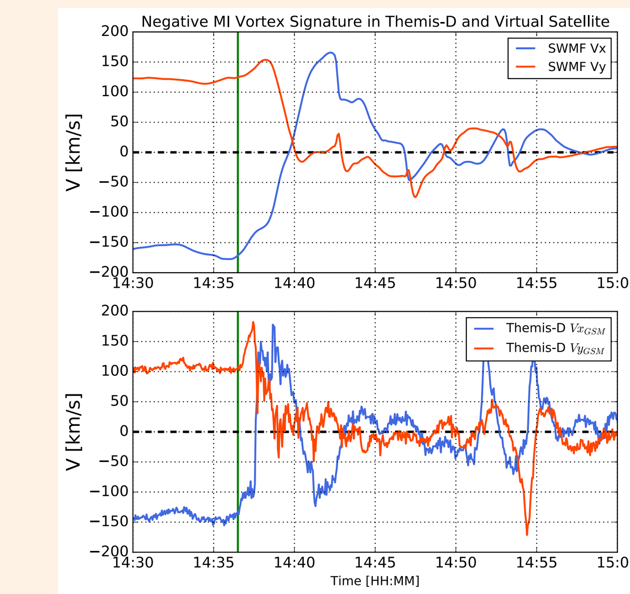

Figure 8: The V_X (blue) and V_Y (red) values obtained from the virtual satellite (upper panel) and the Themis-D satellite (bottom panel) are shown. The green line marks 1437 UT, the arrival of the negative pressure pulse.

6. CONCLUSIONS AND FUTURE WORK

We studied the 11 June 2017 SI- event to understand how the expansion affects the coupled M-I-T system. We used the ionospheric electrodynamic potential and auroral power derived from the self-consistent global MHD model (BATS-R-US) to drive the I-T model (GITM). Our major findings are listed below:
- The expansion of the geospace system created a two step response: Negative PI and MI phases.
- An **upward FAC on dusk** and a **downward FAC on dawn** formed during the negative PI phase with peaks around 0.1 $\mu A/m^2$.
- A **downward FAC on dusk** and **an upward FAC on dawn** formed during the negative MI phase that had slightly smaller amplitudes compared to negative PI FACs.
- Perturbation FACs that formed during the expansion were **weaker** compared to the ones formed during compression.
- Ground magnetic perturbation at lower latitudes showed **a stepwise decrement** due to the expansion of the magnetosphere system.
- The vortices that were created during the expansion phase **did not modify the ion convection** patterns strongly.
- The ion temperature enhancement was around **400 K**, which is lower compared to that of a compression event which can exceed 1000 K [Ozturk et al., 2018].
- The brief southward turning of the IMF B_Z proved to be a much more significant source of perturbation for the ion convection patterns.
- The thermospheric temperature enhancement during expansion was **below 10K** on the dayside region near 11 LT.

We will further investigate the effects of solar wind and IMF drivers through idealized simulations to comparetively understand their effects on the M-I-T system.

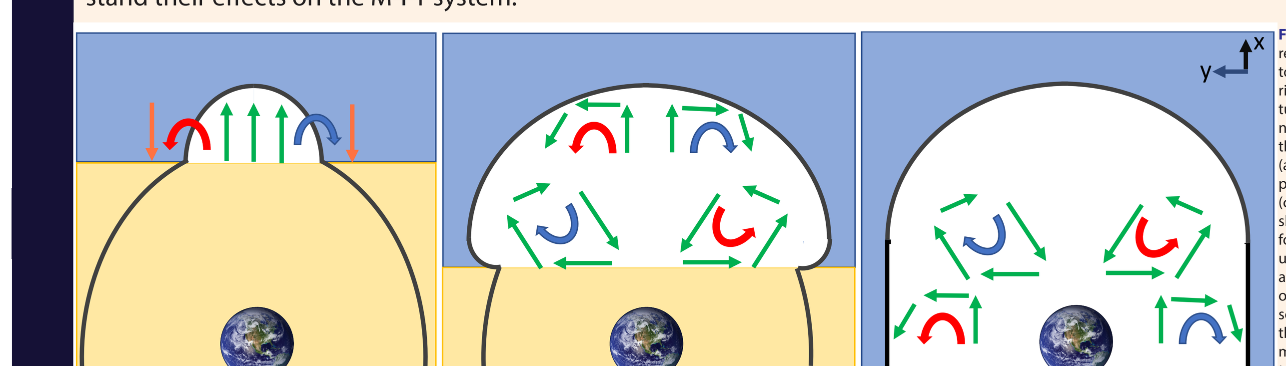

Figure 9: A schematic representation of the magnetospheric sources that give rise to PI- and MI- signatures at the ground magnetometers are shown at the beginning of PI- phase (a), the beginning of MI- phase, and late MI- phase (c). The red (blue) arrows show the sense of rotation for the vortex and the upward (downward) FAC associated with it. The orange arrows show the solar wind velocity vectors, the green arrows show mangetospheric flow vectors.

7.REFERENCES

Araki, T. and H. Nagano, (1988), Geomagnetic response to sudden expansions of the magnetosphere, Journal of Geophysical Research, vol.93, 3983-3988
Araki, T. (1994), A physical model of the geomagnetic sudden commencement, Solar wind sources of magnetospheric ULF waves
Ozturk , D. S., S. Zou, A. J. Ridley, J. A. Slavin, (2018), Modeling study of the geospace system response to solar wind dynamic pressure enhancement on March 17, 2015, Journal of Geophysical Research
Ridley, A. J., Y. Deng, G. Toth (2006), The global ionosphere-thermosphere model (GITM), Journal of Atmospheric Solar-Terrestrial Physics, 68, 839-864
Sato, N., Y. Murata, H. Yamagishi, A. S. Yukimatu, M. Kikuchi, M. Watanabe, K. Makita, H. Yang, R. Liu, F. J. Rich, (2001), Enhancement of optical aurora triggered by the solar wind negative pressure impulse (SI-), Geophysical Research Letters, vol.28, 127-130
Toth, G., I. V. Sokolov, T. I. Gombosi, D. R. Chesney, C. R. Clauer, D. L. De Zeeuw, K. C. Hansen, K. J. Kane, W. B. Manchester, R. C. Oehmke, K. G. Powell, A. J. Ridley, I. I. Roussev, Q. F. Stout, O. Volberg, (2005), SWMF, Journal of Geophysical Research, 110, A12226
Zhao, H. Y., X. C. Shen, B. B. Tang, A. M. Tian, Q. Q. Shi, J. M. Weygand, Z. H. Yao, G.-G. Zong, S. Y. Fu, S. T. Yao, T. Xiao, Z. Y. Pu, (2016), Magnetospheric vortices and their global effect after a solar wind dynamic pressure decrease, Journal of Geophysical Research, vol.121, 1071-1077

8. ACKNOWLEDGEMENTS

The authors would like to acknowledge high-performance computing support from Yellowstone (ark:/85065/d7wd3xhc) provided by National Center for Atmospheric Research (NCAR) Computational and Information Systems Laboratory, sponsored by the National Science Foundation, the University of Michigan Center for Space Environment Modeling and the SpacePy Team. Author Dogacan Ozturk thanks to Darren DeZeeuw, Yuxi Chen, Daniel Welling and Xianzhe Jia for their useful comments. This work was supported by NSF Grant no: AGS1203232. This research has made use of NASA's Astrophysics Data System. For the ground magnetometer data we gratefully acknowledge: Intermagnet; USGS, Jeffrey J. Love; CARISMA, PI Ian Mann; CANMOS; The S-RAMP Database, PI K. Yumoto and Dr. K. Shiokawa; The SPIDR database; AARI, PI Oleg Troshichev; The MACCS program, PI M. Engebretson, Geomagnetism Unit of the Geological Survey of Canada; GIMA; MEASURE, UCLA IGPP and Florida Institute of Technology; SAMBA, PI Eftyhia Zesta; 210 Chain, PI K. Yumoto; SAMNET, PI Farideh Honary; The institutes who maintain the IMAGE magnetometer array, PI Eija Tanskanen; PENGUIN; AUTUMN, PI Martin Connors; DTU Space, PI Dr. Rico Behlke; South Pole and McMurdo Magnetometer, PI's Louis J. Lanzarotti and Alan T. Weatherwax; ICESTAR; RAPIDMAG; PENGUIn; British Artarctic Survey; McMac, PI Dr. Peter Chi; BGS, PI Dr. Susan Macmillan; Pushkov Institute of Terrestrial Magnetism, Ionosphere and Radio Wave Propagation (IZMIRAN); GFZ, PI Dr. Juergen Matzka; MFGI, PI B. Heilig; IGFPAS, PI J. Reda; University of L'Aquila, PI M. Vellante; BCMT, V. Lesur and A. Chambodut; Data obtained in cooperation with Geoscience Australia, PI Marina Costelloe; SuperMAG, PI Jesper W. Gjerloev.